Catal Lett (2012) 142:492–500
DOI 10.1007/s10562-012-0782-8

Synthesis of 2-Methylpyrazine Over Highly Dispersed Copper Catalysts

Wen Luo · Fang-Li Jing · Xiao-Peng Yu · Si Sun · Shi-Zhong Luo · Wei Chu

Received: 3 November 2011 / Accepted: 13 February 2012 / Published online: 7 March 2012

Abstract A series of CuCoAl catalysts were synthesized by co-precipitation and impregnation methods, tested in synthesis of 2-methylpyrazine (2-MP) and characterized by X-ray diffraction, N_2 adsorption, thermo-gravimetry analysis, H_2-temperature-programmed reduction, dissociative N_2O adsorption and temperature-programmed oxidation. The precursors prepared by co-precipitation method shows a well-crystallized hydrotalcite. The study proves that the calcination temperature of hydrotalcite has a significant effect on the catalyst surface area, crystallite size and copper dispersion. In comparison with catalyst prepared by impregnation, the catalyst prepared by co-precipitation method calcined at 500 °C exhibits higher specific surface area, higher copper dispersion and the better reducibility. Consequently, CuCoAl catalyst derived from hydrotalcite is more active and selective for synthesis of 2-MP. Moreover, it shows the better stability due to the good resistance to coke formation.

Keywords CuCoAl catalyst · 2-Methylpyrazine · Hydrotalcite · High dispersion

1 Introduction

Supported copper catalysts are widely used in many reactions, including methanol steam reforming [1–3], methanol oxidation steam reforming (OSRM) [4, 5], ester hydrogenolysis [6, 7], and selective catalytic reduction of NO_x [8, 9]. It is generally accepted that decreasing the copper particle size can increase the number of reactive sites on the surface of the catalyst, which is an efficient way to improve the catalytic activity. For the application of copper nanoparticles as catalysts, it is desirable to prepare highly dispersed and nano-sized copper particles on a support surface. Conventional methods, such as impregnation, ion-exchange, co-precipitation and sol–gel methods are applied to prepare highly dispersed cooper catalyst. However, disadvantages have been reported in some articles [10–12]. Inhomogeneous agglomeration of copper species often occurs, especially at higher content for impregnation method, and which results in large-sized copper particles [10]. Although the ion-exchange method gives a better dispersion of copper [11], it cannot be widely used for the low loading of active species; while for some sol–gel catalysts, lower activities are usually observed due to encapsulation of activity phase [12].

Hydrotalcite-type compounds (HTls), a class of layered materials, are receiving considerable attention in recent years owing to their diverse applications [13–17]. The general formula of HTls is $\left[M^{II}_{1-x}M^{III}x(OH)_2\right]^{x+}\left[A^{n-}x/n\right]^{x-}\cdot mH_2O$ where M^{II} and M^{III} are di- and trivalent metals, respectively, the value of x is equal to the mole ratio of $M^{III}/(M^{III}+M^{II})$ and A^{n-} is an anion. Thermal decomposition of HTls leads to the formation of homogeneous mixed metal oxides with high metal dispersion, high surface area, high thermal stability, etc., which are essential for the material to function as a promising catalyst. Moreover, materials with desired properties can be perceived from decomposition of HTls which contain proper transition metal ions in the lattice. In particular, calcining the Co–Al containing HTls precursors usually

W. Luo · F.-L. Jing · X.-P. Yu · S. Sun · S.-Z. Luo (✉) · W. Chu (✉)
Department of Chemical Engineering, Sichuan University, Chengdu 610065, China
e-mail: luoszscu@gmail.com

W. Chu
e-mail: chuwei65@yahoo.com.cn

obtains Co–Al spinels or the mixed oxides with high surface area [18, 19]. Due to its unique chemical and physicochemical properties, such as high thermal stability, high mechanical resistance, and low surface acidity, Co–Al spinel and the mixed oxides have been studied as a heterogeneous catalyst in the capture and decomposition of nitrous oxide [18, 20], hydroxylation of phenol [21] and oxidation of CO [22]. Rives et al. [21] and Velu et al. [23] have prepared Cu–Co–Al and Cu–Co–Zn–Al hydrotalcites, respectively, and focused on the effect of cobalt on the nature of crystalline phases. However, for all of their samples, they maintained the atomic ratio of the M^{II}/M^{III} at around 3.0, which can form the pure HTls phase. Wide range of the atomic ratio and, in particular, the state of copper in the mixed oxides obtained by thermal decomposition from HTls at different temperature should be further studied.

2-Methylpyrazine (2-MP) is an intermediate compound for the synthesis of 2-amidopyrazine, which is a well-known bacteriostatic and antitubercular drug. In recent years, 2-MP is mostly synthesized by cyclization of ethylenediamine (ED) and 1,2-propylene glycol (PG) [24, 25]. As far as we know, most recent works were mainly drawn on the study of catalytic activity and 2-MP yield over different solid acid catalyst systems (e.g., Al_2O_3). However, Al_2O_3 has poor anti-coking performance and hydrothermal stability. Therefore, CuCoAl spinel like catalysts with high thermal stability and low surface acidity were chosen as a kind of catalyst to synthesize 2-MP.

In this paper, we will report another method to obtain highly dispersed copper catalysts through thermal decomposition of Cu–Co–Al hydrotalcite-like compounds. Highly dispersed copper catalysts carried on nano-sized Co–Al spinel with a large surface area and high stability can be obtained through controlling the calcination temperature of the HTls precursors. The catalysts are tested in the synthesis of 2-MP, and characterized by a variety of means, including N_2-adsorption/desorption, X-ray diffraction (XRD), TG-DTG, H_2-temperature-programmed reduction (H_2-TPR), N_2O adsorption, and O_2-TPO.

2 Experimental

2.1 Catalysts Preparation

The CuCoAl precursor (Cu:Co:Al = 1:1:4, mole ratio) was prepared by the traditional Na_2CO_3/NaOH co-precipitation method [20]. 100 mL mixed metal solution containing 1 M of total cations concentration of $Cu(NO_3)_2{\cdot}6H_2O$, $Co(NO_3)_2{\cdot}6H_2O$, $Al(NO_3)_3{\cdot}9H_2O$, with the desired molar ratio and 100 mL mixed basic solution consisting of NaOH and Na_2CO_3 with $[OH^-] = 2.0$ mol/L and $[OH^-]/[CO_3^{2-}] = 2$ were simultaneously added dropwise into 100 mL distilled water under vigorous mechanical stirring. The mixed solution was kept at constant pH (10 ± 0.5). The resulting suspension was aged in the mother liquor at 70 °C for 12 h. Then, the solid were obtained by thoroughly washing with distilled water, dried at 70 °C for 12 h and further at 120 °C overnight. Finally the precursors were calcined at 500, 600, and 800 °C for 4 h, designated as CCA-500, CCA-600, and CCA-800, respectively.

For comparison, a reference sample with same composition (Cu:Co:Al = 1:1:4, mole ratio) was prepared by wet impregnation. γ-Al_2O_3 (BET surface area = 250 m^2/g, 40–60 mesh) was used as the catalyst supports. The support was preheated at 400 °C to remove the adsorbed water. Then the required amount of an aqueous solution of $Cu(NO_3)_2{\cdot}3H_2O$ and $Co(NO_3)_3{\cdot}6H_2O$ was slowly added to the support, with thoroughly stirring at room temperature. The precursors were dried at 120 °C overnight and calcined at 500 °C for 4 h. The resulting sample was assigned as CCA-IM.

2.2 Catalyst Characterization

All the XRD experiments were performed on a Philips X' pert PRO powder diffractometer with graphite-monochromated Cu Kα radiation in the Bragg–Brentano parafocusing geometry. The patterns were collected between 10° and 80° (2θ range), with scanning speed at 10°/min.

The specific surface area, total pore volume and average pore diameter were determined by N_2 adsorption/desorption isotherms at −196 °C, using Quantachrome NOVA 1000e apparatus. Before each measurement, the sample was degassed in vacuum at 300 °C for 3 h.

The hydrotalcite-like precursors were measured with a thermo-gravimetric analyzer thermo-gravimetry analysis (TGA Q500). The sample was heated in air flow from room temperature to 800 °C at a heating rate of 10 °C/min.

Temperature-programmed reduction (TPR) experiments were carried out in a fixed-bed reactor. 50 mg catalyst was reduced with a 5% H_2/N_2 mixed gas (30 mL/min) from 100 to 900 °C at a rate of 10 °C/min. The hydrogen consumption was analyzed on-line by a SC-200 gas chromatograph with a thermal conductivity detector (TCD). The amounts of hydrogen consumption were calibrated by using known amounts of CuO.

The copper surface area and dispersion were measured by dissociative N_2O adsorption at 50 °C [16, 26]. 50 mg catalyst was pre-reduced at 180 °C (with a heating rate of 5 °C/min) for 1 h in 5% H_2/N_2 mixture gas flow (30 mL/min). Then, the temperature was cooled to 50 °C in N_2 and exposed to 25% N_2O/N_2 (40 mL/min) for 30 min to make the reduced surface Cu atoms oxidized to Cu_2O. After that, the catalyst was purged with N_2 to remove the oxidant. The second TPR was carried out from 50 to 180 °C at a rate of 5 °C/min and hold at 180 °C

for 1 h to reduce Cu_2O to Cu. Copper dispersion (D_{Cu}), defined as the ratio of Cu exposed at the surface to total Cu, and was calculated from the amount of H_2 consumed of $Cu_2O \rightarrow Cu$. Cu metal surface area (MSA) was calculated as: MSA (m^2/g-Cu) = $MolH_2 \cdot SF \cdot N_A / 10^4 \cdot C_M \cdot W_{Cu}$, where $MolH_2$, SF, N_A, C_M, and W_{Cu} are = moles of hydrogen experimentally consumed per unit mass of catalyst ($\mu mol_{H_2} g/cat$), stoichiometric factor (SF = 2 for our cases), Avogadro's constant (6.022×10^{23}/mol), number of surface Cu atoms per unit surface area (1.47×10^{19} atoms/m^2), and Cu content (wt%), respectively. Average copper particle size was calculated as: d (nm) = $10^7 \cdot SK \cdot C_M \cdot W_{Cu} / SF \cdot MolH_2 \cdot \rho_{Cu}$, where SK is a constant depending on Cu particle shape (6 or 5) and ρ_{Cu} is the density of copper (8.92 g/cm^3). The error in the Cu surface area data was estimated to be less than 10%.

Temperature-programmed oxidation (TPO) experiments were carried out in a fixed-bed reactor. 30 mg of the spent catalyst was loaded, and the reaction gas of 5% O_2/Ar with a flow rate of 50 mL/min was introduced. The temperature of the reactor was raised from 100 to 600 °C at a heating rate of 10 °C/min controlled by a temperature controller. The products were analyzed on-line by a Hiden QIC-20 mass spectrometer.

2.3 Catalytic Test

Catalytic activity test was carried out at atmospheric pressure in a continuous fixed-bed reactor, 0.5 g of catalyst was loaded at the middle of the tube (Quartz, inner diameter = 8 mm, length = 300 mm). Before reaction, the catalyst was reduced under the H_2 and N_2 gas mixture flow (H_2/N_2 = 1, molar ratio) at 400 °C for 1 h. The liquid feed, prepared by mixing ED and PG in the mole ratio of 1:1, diluted with deionized water (50 wt%), was injected into reactor by a micro pump at 5 mL/h and N_2 (25 mL/min) was supplied as a carrier gas. The liquid products were collected in an ice-water condenser and analyzed by gas chromatography (GC-112A) with a capillary column (cross-linked SE-30 gum, 0.33 mm × 30 m) and flame ionization detector (FID).

3 Results and Discussion

3.1 Hydrotalcite-Like Precursors and the Thermal Decomposition Behaviors

Figure 1 shows the XRD pattern of CuCoAl precursor (CCA-HT). It can be seen that the precursor is a typical hydrotalcite-like phase with sharp diffraction peaks at 2θ = 11.8°, 23.6°, and 34.9°, corresponding to the reflection of crystalline planes of (003), (006), and (009), respectively. The in-plane XRDs from planes (110) and

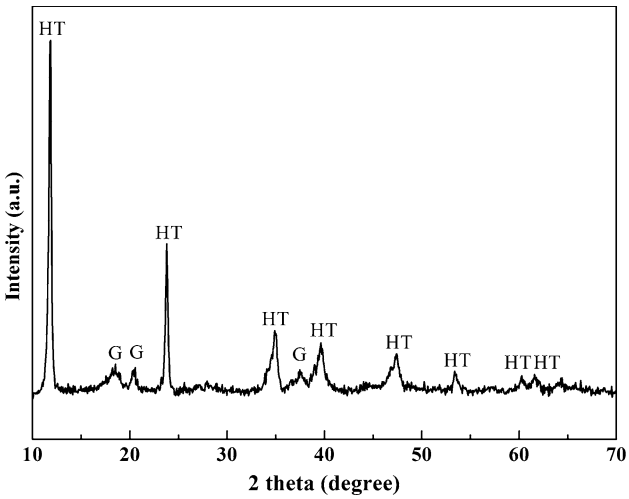

Fig. 1 XRD patterns of CCA-HT sample (*HT* hydrotalcite, *G* gibbsite)

(113) can be also noted at 60.3° and 61.6°, respectively. Many authors [22, 27] reported that it is possible to obtain single stoichiometric HTls phases in the range of $M^{III}/(M^{III} + M^{II})$ = 0.2–0.4. For our case, the ratio of $Al^{3+}/(Al^{3+} + Cu^{2+} + Co^{2+})$ is 0.67, which is considerably higher than the referred value above. Pérez-Bernal et al. [28] found that the excess amount of aluminum in the Co(Zn)–Al HTls samples is segregated forming the additional phases, instead of incorporating into the hydrotalcite-type structure or changing the structure. Hence, it suggests that it is possible to obtain the other crystallite phases besides the HTls. As a result, the impurity phases of gibbsite phase $Al(OH)_3$ (JCPDS file 033-0018) is observed from the XRD diffraction patterns.

The thermal-gravimetric analysis (TG/DTG) curves are shown in Fig. 2. It can be observed that CCA-HT precursor exhibits four weight loss courses. The first weight loss below 120 °C is ascribed to removal of physically adsorbed water. The second weight loss, identified by a DTG peak at 200 °C, corresponds to the loss of interlayer water molecules.

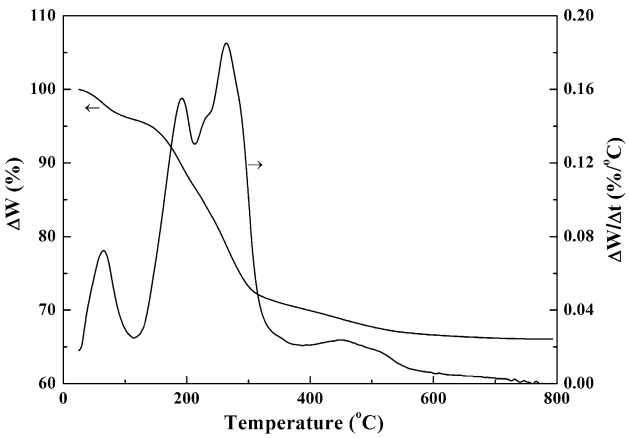

Fig. 2 TG and DTG of CCA-HT sample

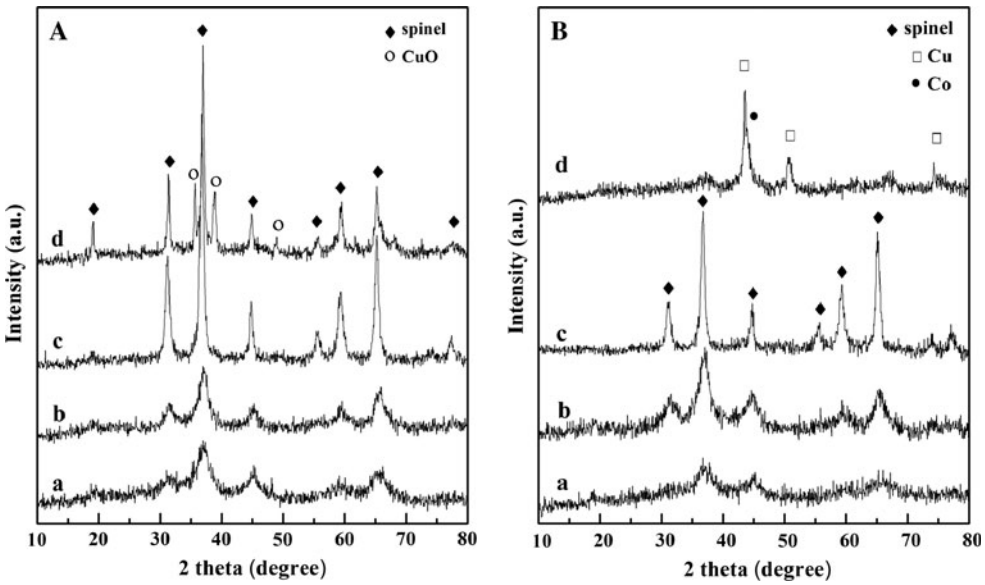

Fig. 3 XRD patterns of **a** as-prepared samples, and **b** reduced samples. *a* CCA-500, *b* CCA-600, *c* CCA-800, and *d* CCA-IM

The third progress, which is displayed as the highest peak at around 270 °C on the DTG curve, is usually attributed to dehydroxylation of brucite-like layers and decarbonylation of the interlayer [14, 29]. For Mg, Al-containing HTls, the weight loss processes are usually included in the above three processes, and generally no further weight loss is recorded above 500 °C. Unlike the HTls built up by Mg and Al, a broad peak in the range 400–550 °C could be observed on the DTG curve, which probably results from the presence of some carbonate ions strongly held to the brucite-like sheets, as discussed elsewhere for other Cu containing hydrotalcite-like materials [21, 30].

3.2 XRD Analysis

The XRD patterns of calcined samples are presented in Fig. 3a. Three samples prepared by co-precipitation method (CCA-CP) show typical spinel phases with diffraction peaks at 32°, 37°, 45°, 51°, 59°, and 65°. With increasing calcination temperature, the intensities of these peaks increase, suggesting that the crystallinity of the spinel phase improves and the crystallite size increases. Taking into account the chemical composition of the precursors (Cu:Co:Al atomic ratio = 1:1:4) and the calcined atmosphere (static air), the formation of Co_3O_4, $CoAl_2O_4$, Co_2AlO_4, $CuAl_2O_4$ and non-stoichiometric Cu–Co spinels ($Cu_{0.76}Co_{2.24}O_4$, $Cu_{0.92}Co_{0.08}O_4$ and $(Cu_{0.3}Co_{0.7})Co_2O_4$) are all possible. However, due to the closeness of the lattice constants of these spinels, it is extremely difficult to ascertain the precise spinel existing in each sample. No diffraction peaks of CuO phase are visible for the co-precipitation samples, probably because CuO is highly dispersed on the catalyst and/or the formation of Cu spinels ($CuAl_2O_4$, $Cu_xCo_{3-x}O_4$).

For the CCA-IM catalyst, the similar diffraction peaks of the spinel phases are also observed in Fig. 3a. As discussed above, it is not clear that these peaks are assigned to Co_3O_4, Cu–Al and/or Co–Al spinel phases. But the strong reflections from CuO are obvious. Comparing to the samples that derived from HTls, inhomogeneous agglomeration of copper species often occurs on the impregnated samples, which results in large-sized CuO particles [10].

The XRD patterns of the samples reduced at 400 °C are shown in Fig. 3b. It is well-known that the Co–Al and Cu–Al spinel phases are difficult to be reduced [23]. Therefore, no obvious change can be seen for the spinel phases after reduction treatment. Diffraction peaks of metallic Cu could not be observed in the reduced CCA-CP catalysts, which indicates that small-sized Cu particles are well dispersed on spinel base or Cu^{2+} formed the stable spinel phase. As far as the sample CCA-IM is concerned, great changes take place after reduction. The metallic Cu is detected as expected. In addition, the disappearance of ill-defined diffraction peaks at 15°, 32°, 37°, 45°, 51°, 59°, and 65° and simultaneously the existence of diffraction peak at 44° ascribed to metallic Co confirm that the Co_3O_4 is formed in the impregnated sample rather than other type of spinel phases [22].

3.3 Textural Properties

All the CCA-CP samples show nitrogen adsorption/desorption isotherms of type II (not shown here), according to IUPAC classification [31]. The curves show a rather narrow hysteresis loop, corresponding to type H3, ascribed to mesopores open at both ends, probably slit-like pores in these samples. The micropores in these catalysts probably arise from micro holes and "chimneys" formed in the

Table 1 Surface area and pore parameters of as-prepared CuCoAl samples

Samples	Surface area[a] (m^2/g)	Pore diameter[b] (nm)	Pore volume[c] (cm^3/g)
CCA-500	185	5.3	0.25
CCA-600	137	4.9	0.17
CCA-800	123	4.8	0.15
CCA-IM	112	4.2	0.12

[a] BET specific areas

[b] Average pore diameter calculated by BJH method

[c] Total pore volumes were obtained at $P/P_0 = 0.975$

brucite-like layers as a consequence of CO_2 and water evolution during calcination, as previously reported [21]. BET surface area, pore volume, and average pore size of all the investigated samples (calculated from their adsorption isotherms) are summarized in Table 1. It can be seen that the surface of the catalysts prepared by co-precipitation method displayed a decrease trend as the calcination temperature increased from 500 to 800 °C. As discussed in XRD, the hydrotalcite-like precursor may transform into spinel phases after thermal treatment. The strong interaction between the metal oxides makes individual crystallite aggregate to form spinel phases having larger size, which are responsible for the decrease in surface area. On the other hand, the similar variations are also found for the pore volume and pore diameter, which indicates that the pore structure of the catalysts are affected by the pronounced increase in particle sizes [32]. Nevertheless, these catalysts show much higher surface area than those spinels obtained from sol–gel methods [33, 34]. Furthermore, the BET surface area of CCA-IM (112 m^2/g) decreases compared to that of Al_2O_3 (250 m^2/g), which is due to the pore blockage by the metal oxides particles.

3.4 H_2-TPR Characterization

H_2-temperature-programmed reduction profiles of the catalysts are shown in Fig. 4. A sharp, intense and symmetrical reduction peak (even a shoulder for CCA-800 sample) at 200 °C is detected in each CCA-CP catalyst. This hydrogen consumption could be attributed to the reduction of CuO to Cu [21]; the shoulder peak in CCA-800 may be due to the reduction of CuO which has strong interaction with the support. The area of this peak decreases with the increase of calcination temperature. This illustrates that the Cu^{2+} formed a more stable spinel structure when the fresh solid was calcined at high temperatures. Apart from these sharp reduction peaks, broad and weak peaks can also be observed at high temperature for all three samples. The broad peaks during the range of 350–800, 350–800, and 450–900 °C for the samples CCA-500, CCA-600 and

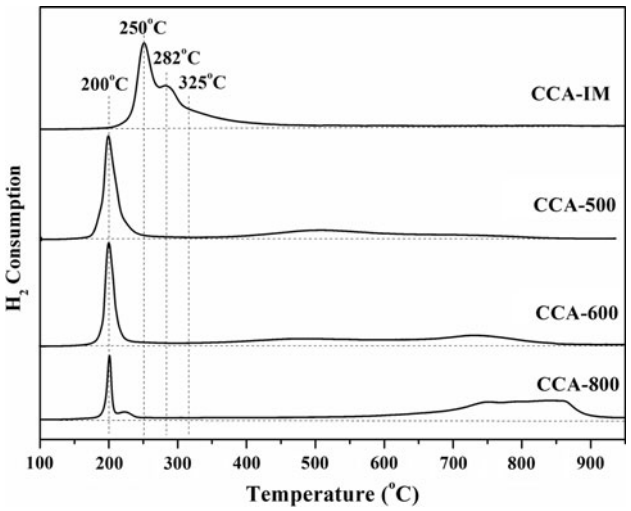

Fig. 4 TPR profiles of as prepared samples

CCA-800, respectively, implies a more difficult reduction caused by the spinel phases [21, 35].

In contrast, quite different profiles could be observed for the CCA-IM sample. Three overlapped peaks between 200 and 450 °C could be found in Fig. 4, which suggests the complicated reduction process. From XRD results, it can be found that CuO and Co_3O_4 are the main reducible metal oxides. Thus, the first peak at ca. 250 °C could be due to the reduction of CuO to Cu, and the other two overlaps at the higher temperatures are attributed to the reduction of Co_3O_4 to Co, consisting of two steps $Co_3O_4 \rightarrow CoO \rightarrow Co$ which are almost indistinguishable [36, 37].

In addition, the reduction peak of pure CuO occurs at around 350 °C (not shown here). For CCA-IM catalyst, a H_2 consumption peak by CuO shows at 250 °C, which is due to that Co^{n+} in the catalyst promotes the reducibility of CuO [23]. But for CCA-CP samples, the CuO reduction peaks appear at 200 °C, which is even lower than that of CCA-IM. Therefore, Co^{n+} is not the only reason for the enhancement of copper reducibility in CCA-CP samples. Some authors found that highly dispersed CuO gave TPR signals at much lower temperatures than bulk CuO [38, 39]. Yuan et al. [16] obtained the copper catalyst through decomposition of Cu–Mg–Al HTls which could be reduced at a low temperature due to the high dispersion of Cu^{2+}. Thence, the high dispersion of CuO in CCA-CP catalysts is another reason of enhancing the CuO reducibility. Moreover, highly dispersed CuO is also one reason for the absence of CuO crystallite in the XRD results.

The amounts of hydrogen consumption for CuCoAl catalysts are shown in Table 2. Compared to theoretical H_2 consumption of $Cu^{2+} \rightarrow Cu^0$, the sharp peak at 200 °C of CCA-500 sample consumes the same amount of H_2, which means nearly all of the Cu^{2+} in CCA-500 are in the form of

Table 2 Hydrogen consumption of CuCoAl catalysts

Samples	H_2 consumption (mmol)		H_2/(Cu + 1.25Co)
	CuO → Cu	Total	
CCA-500	0.146	0.297	0.94
CCA-600	0.116	0.295	0.94
CCA-800	0.041	0.262	0.83
CCA-IM	0.141	0.310	0.98

Theoretical H_2 consumption of $Cu^{2+} \rightarrow Cu^0$ is 0.140 mmol

CuO. At the same time, spinels in this catalyst should be attributed to $CoAl_2O_4$ and/or Co_2AlO_4. With increasing calcination temperature, more and more Cu^{2+} are not in the form of CuO as described above, meaning that $CuAl_2O_4$ or/and Cu–Co spinels formed in the CCA-600 and CCA-800 catalysts. This explains the increment of number and area of reduction peak at high temperatures in these two samples. Considering that the oxidation state of Co^{n+} may be Co^{2+} and Co^{3+}, we assume that the average oxidation state is $Co^{2.5+}$. The ratios of the amount of H_2 consumed to that required for complete reduction of Cu^{2+} and $Co^{2.5+}$ are also summarized in Table 2. For CCA-500, CCA-600, and CCA-IM, the ratios are close to 1.0, indicating that the average oxidation state of cobalt ions in these three catalysts are close to 2.5. The ratio of H_2/(Cu + 1.25Co) for CCA-800 is only 0.83, which may be due to that the oxidation of Co ions is close to 2.0 and/or a low reduction degree caused by the high calcination temperature.

3.5 Copper Dispersion Measurements

The Cu surface area, Cu dispersion and surface Cu crystallite size of the reduced samples, measured by N_2O chemisorptions, are shown in Table 3. In this experiment, the pre-reduction temperature was selected at 180 °C, and the reduction of Co^{n+} at such a low temperature is found to be negligible, hence the N_2O chemisorptions is attributed to surface Cu atoms. In addition, the mild conditions used for pre-reduction were effective for reducing the CuO phase to Cu but they did not allow reducing the formed Cu–Al and Cu–Co spinels. The similar situation has been studied by Gervasini et al. [26]. They pointed out that when using the peak areas in first TPR profile to represent the total amount of Cu^{2+} in the sample, non-quantitative reduction of Cu^{2+} to Cu will lead to underestimation of total Cu^{2+} and then overestimation of copper dispersion. Therefore, we could not get the precise amount of Cu^{2+} from the first TPR profile. In this condition, the values of Cu dispersion have been related to the total Cu content and so can be considered as nominal as has been reported by Esposito et al. [40]. Nevertheless, it can be found that the dispersion of copper in reduced CCA-500 and CCA-600 catalysts are very high, which reaches 72.0 and 64.3%, respectively. Although the calcination temperature of CCA-800 catalyst reaches 800 °C and most of the Cu^{2+} enter into the spinel structure, the remained Cu^{2+} still exist in a highly dispersed form. Cu crystallite sizes of CCA-CP samples are all below 2 nm, which explains the absence of Cu diffraction peak in XRD patterns of reduction samples. Catalyst prepared by impregnation method shows lower Cu surface area than that of catalysts obtained by the decomposition of hydrotalcite-like precursors, as it can be seen that the Cu surface area of reduced CCA-IM sample is only 136.6 m^2/g-Cu.

Table 3 Cu dispersion in reduced CuCoAl catalysts

Samples	Dispersion (%)	Cu surface area (m^2/g-Cu)	Cu crystallite size[a] (nm)
CCA-500	72.0	462.0	1.4
CCA-600	64.3	412.5	1.6[b]
CCA-800	23.9	153.3	4.3[b]
CCA-IM	21.3	136.6	4.9

[a] Calculated with $SK = 6$ (spherical or cubic shape of the Cu aggregates)

[b] Certain amount of Cu^{2+} in spinel phase could not be reduced during this experiment, leading to overestimation of Cu crystal size [26], corrected data for both of CCA-600 and CCA-800 are ca. 1.3 nm

3.6 Catalytic Performance and Coke Deposition

3.6.1 Synthesis of 2-MP on Different Catalysts

The catalytic performances over the prepared CuCoAl catalysts for synthesis of 2-MP are summarized in Table 4. All of the CuCoAl catalysts show high activity at an extremely high WHSV (10 h^{-1}); the conversion of PG and ED reaches 96 and 86%, respectively. However, the selectivity to 2-MP of these catalysts shows obvious difference. CCA-500 catalyst exhibits the best selectivity to 2-MP which reaches 57.8%. With the increase of calcination temperature, the selectivity decreases quickly, especially for CCA-800 catalyst. Park et al. [41, 42] reported

Table 4 Synthesis of 2-MP on reduced CuCoAl catalysts

Catalyst	Conversion (%)		2-MP Selectivity (%)
	ED	PG	
CCA-500	86.0	99.2	57.8
CCA-600	86.5	96.3	54.5
CCA-800	86.9	96.6	34.0
CCA-IM	85.0	97.6	46.1

Reaction conditions: 0.5 g catalyst, temperature = 400 °C, reaction time = 2 h, WHSV = 10 h^{-1}

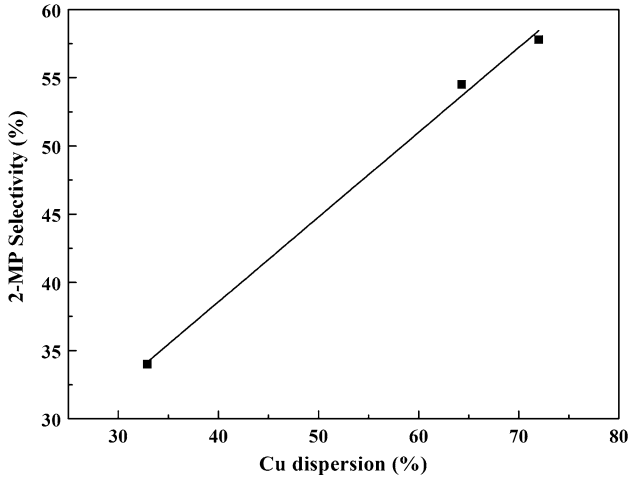

Fig. 5 Cu dispersion of CCA-CP samples versus the selectivity to 2-MP

metal (Cu, Co, Ni) oxide-modified ZnO/SiO_2 for cyclo-dehydrogenation of ED with PG to 2-MP and demonstrated that metallic site of catalyst was responsible for the dehydrogenation of 2-methylpiperzine to 2-methylpyrazine. The pre-reduction treatment of the catalysts is carried at 400 °C, little Co^{n+} and most of the CuO in the CCA-CP samples are reduced to metallic sites as evidenced by TPR results, which means Cu^0 has the main contribution to the selectivity to 2-MP. Figure 5 shows the correlations of 2-MP selectivity with Cu dispersion of CCA-CP catalysts. A strong correlation ($R^2 = 0.993$) between 2-MP selectivity and Cu dispersion allows us to regard it as a liner relationship. Therefore, it can be confirmed that the amount of metallic Cu on catalyst surface plays a decisive role in the 2-MP selectivity and highly dispersed copper catalyst is necessary for synthesis of 2-MP.

At the pre-reduction temperature of 400 °C, Co_3O_4 and CuO are completely reduced to metallic centers in the CCA-IM catalyst. Metallic Co is also dehydrogenation center in synthesis of 2-MP [42]. Nevertheless, due to the lager crystallite size and smaller MSA, the selectivity to 2-MP is still lower than CCA-500 and CCA-600.

3.6.2 *Stability Test*

Figure 6 compares the conversion of ED and PG, and the selectivity to 2-MP as a function of time on stream at 400 °C on the CCA-500 and CCA-IM catalysts. The CCA-IM catalyst shows a really poor stability. With time on stream, the conversion of ED and PG decreases rapidly to 50 and 63%, respectively. At the same time, the selectivity to 2-MP also decreases to 25%. In contrast, the CCA-500 catalyst exhibits rather stable performance for 100 h with time on stream. There are no significant variation on the conversion of ED and PG during the stability test. Although the selectivity to 2-MP of CCA-500 catalyst decreases by 10% at the initial 20 h, it remains stable at around 50% in the later 80 h. Compared with γ-Al_2O_3, the improved stability of the CCA-500 catalyst may be caused by the lower surface acidity of spinel, which suppresses coke deposition on the catalyst surface. Moreover, small metal particles well dispersed on catalyst surface may also enhance the stability of the catalysts [17, 43].

3.6.3 *O_2-TPO of Spent Catalysts*

O_2-TPO analysis was performed to investigate the carbon deposition of the spent catalysts. The results are presented in Fig. 7. In order to get more insight into the TPO results, the profiles were deconvoluted by Gaussian shaped

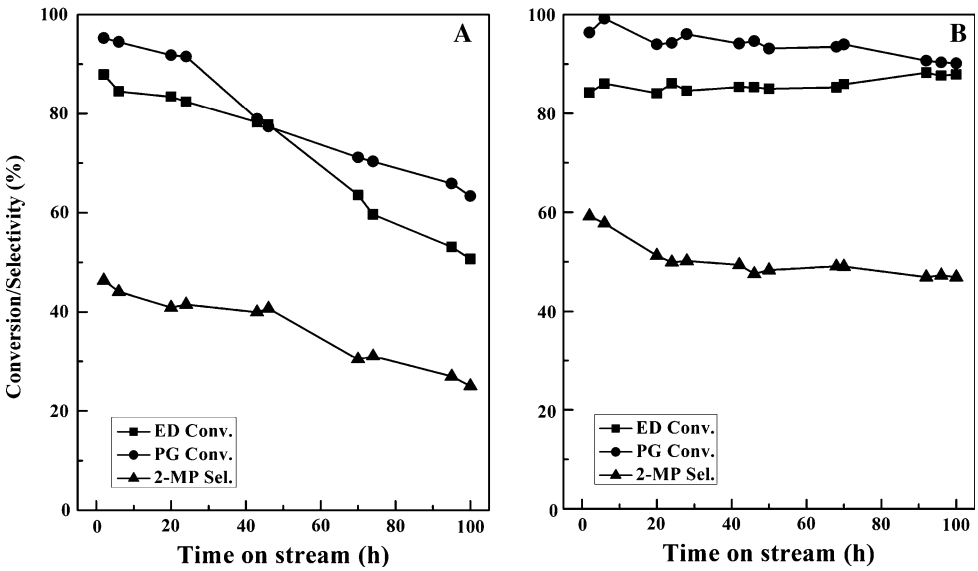

Fig. 6 Evolution of catalytic performances of **a** CCA-IM, and **b** CCA-500 catalysts with time on stream (Reaction conditions: 0.5 g catalyst, temperature = 400 °C, WHSV = 10 h^{-1})

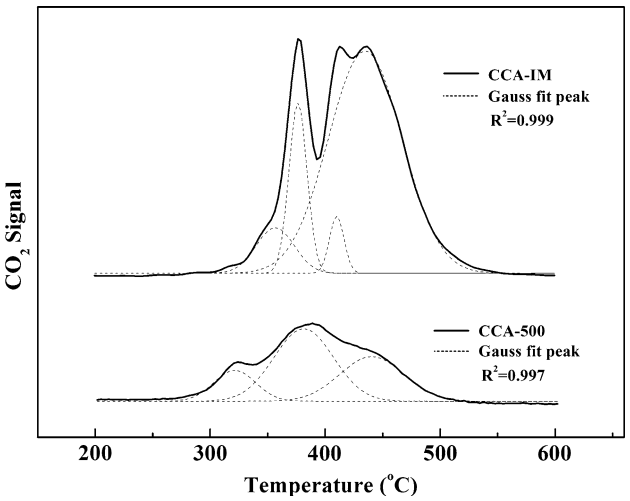

Fig. 7 TPO profiles of CCA-500 and CCA-IM catalysts after 100 h time on stream

function. Three peaks of the TPO curves correspond to three different coke combustion processes. Different TPO components are explained by consumption of coke on different position of catalysts [44–46]. For the spent CCA-500 catalyst, the oxidation peaks at low temperatures centered on 320 °C is ascribed to the carbonaceous material deposited on the Cu metallic sites whose combustion is activated by the metallic sites. The peak at around 380 °C is attributed to coke deposited on the metal-support interface. And the last fraction of coke which requires a higher temperature, between 400 and 500 °C is deposited on the support far from the metallic center and its combustion is not catalyzed. More types of coke deposited on the spent CCA-IM catalyst performed as four TPO components in Fig. 7; it could be studied as three parts. The first two peaks between 300 °C and 400 °C are attributed to coke deposited on metallic centers and near the metal-support interphase. Similar to CCA-500, the peak at above 400 °C belongs to coke deposited on the support.

The amount of coke deposited on CCA-IM catalyst is two times as much as that of the CCA-500 catalyst, which reveals that CCA-500 catalyst has a better resistance to coke deposition during synthesis of 2-MP. This result is probably induced by small Cu particle size and larger Cu surface area; because Christensen et al. [43] considered that smaller metal crystals have a larger saturation concentration level of carbon than larger crystals, which result in a smaller driving force for carbon diffusion.

4 Conclusions

In summary, a novel solid base catalyst containing copper and spinel was prepared by the thermal decomposition of Cu–Co–Al hydrotalcite-like compounds in this work. N_2 adsorption results show that this kind of spinel catalysts exhibit high surface area. XRD, TPR, and N_2O adsorption results indicate that the catalyst calcined at a lower temperature exhibits higher copper dispersion. With increasing calcination temperature, the surface area of the catalyst decreases and the crystallite size of spinel phase increases, meanwhile, the catalyst becomes hard to be reduced due to that more copper are in the form of spinel phase. Therefore, higher activity for synthesis of 2-MP is observed on the catalysts calcined at a lower temperature, especially for CCA-500. Moreover, due to the strong resistance to coke deposition, CCA-500 exhibits a high stability in synthesis of 2-MP.

Acknowledgments This work was supported by the National High Technology Research and Development Program (863 Program, NO.2008AA062402-1), the National Basic Research Program of China Program (973 Program, NO.2011CB201202), and Chinese Chengda Scholarship.

References

1. Agrell J, Birgersson H, Boutonnet M, Melián-Cabrera I, Navarro RM, Fierro JLG (2003) J Catal 219:389
2. Matter PH, Braden DJ, Ozkan US (2004) J Catal 223:340
3. Kniep BL, Girgsdies F, Ressler T (2005) J Catal 236:34
4. Velu S, Suzuki K, Okazaki M, Kapoor MP, Osaki T, Ohashi F (2000) J Catal 194:373
5. Turco M, Bagnasco G, Costantino U, Marmottini F, Montanari T, Ramis G, Busca G (2004) J Catal 228:56
6. Natal-Santiago MA, Sánchez-Castillo MA, Cortright RD, Dumesic JA (2000) J Catal 193:16
7. Scheur FT, Linden B, Mittelmeijer-Hazeleger MC, Nazloomian JG, Staat LH (1994) Appl Catal A Gen 111:63
8. Zawadzki M, Staszak W, López-Suárez FE, Illán-Gómez MJ, Bueno-López A (2009) Appl Catal A Gen 371:92
9. Obalová L, Karásková K, Jirátová K, Kovanda F (2009) Appl Catal B Environ 90:132
10. Takahashi R, Sato S, Sodesawa T, Kato M (2000) J Sol–Gel Sci Technol 19:715
11. Carvalho MCN, Passos FB, Schmal M (2002) Catal Commun 3:503
12. Wang ZL, Liu QS, Yu JF, Wu TH, Wang G (2003) Appl Catal A Gen 239:87
13. Choudary BM, Kantam ML, Rahman A, Reddy CV, Rao KK (2001) Angew Chem Int Ed 40:763
14. Gao LD, Tang Y, Xue QS, Liu Y, Lu Y (2009) Energ Fuels 23:624
15. Zhou CH, Beltramini JN, Lin CX, Xu ZP, Lu GQM, Tanksale A (2011) Catal Sci Technol 1:111
16. Yuan ZL, Wang L, Wang JH, Xia SX, Chen P, Hou ZY, Zheng X (2011) Appl Catal B Environ 101:431
17. Yu XP, Chu W, Wang N, Ma F (2011) Catal Lett 141:1228
18. Yu JJ, Wang XP, Li LD, Hao ZP, Xu ZP, Lu GQM (2007) Adv Funct Mat 17:3598
19. Xu WJ, Liu XH, Ren JW, Liu HH, Ma YC, Wang YQ, Lu G (2011) Microporous Mesoporous Mater 142:251
20. Yu JJ, Tao YX, Liu CC, Hao ZP, Xu Z (2007) Environ Sci Technol 41:1399
21. Rives V, Dubey A, Kannan S (2001) Phys Chem Chem Phys 3:4826

22. Gabrovska M, Edreva-Kardjieva R, Tenchev K, Tzvetkov P, Spojakina A, Petrov L (2011) Appl Catal A Gen 399:242
23. Velu S, Suzuki K, Hashimoto S, Satoh N, Ohashi F, Tomura S (2001) J Mater Chem 11:2049
24. Forni L, Pollesel P (1991) J Catal 130:403
25. Forni L, Stern G, Gatti M (1987) Appl Catal 29:161
26. Gervasini A, Bennici S (2005) Appl Catal A Gen 281:199
27. Holgado MJ, Rivers V, Román MSS (2001) Appl Catal A Gen 214:219
28. Pérez-Bernal ME, Ruano-Casero RJ, Rives V (2009) J Solid State Chem 182:2566
29. Jing FL, Zhang YY, Luo SZ, Chu W, Qian W (2010) Appl Clay Sci 48:203
30. Rives V, Kannan S (2000) J Mater Chem 10:489
31. Sing KSW, Everett DH, Haul RAW, Moscou L, Pierotti RA, Rouquerol J, Siemieniewska T (1985) Pure Appl Chem 57:603
32. Mokhtar M, Basahel SN, Al-Angary YO (2010) J Alloy Compd 493:376
33. Shimoda N, Faungnawakij K, Kikuchi R, Fukunag T, Eguchi K (2009) Appl Catal A Gen 365:71
34. Faungnawakij K, Shimoda N, Tetsuya F, Ryuji K, Eguchi K (2009) Appl Catal B Environ 92:341
35. Lamonier JF, Boutoundou AB, Gennequin C, Pérez-Zurita MJ, Siffert S, Aboukais A (2007) Catal Lett 118:165
36. Wang N, Chu W, Zhang T, Zhao XS (2011) Chem Eng J 170:457
37. Wang N, Chu W, Huang LQ, Zhang T (2010) J Nat Gas Chem 19:117
38. Agrell J, Hasselbo K, Jansson K, Järås SG, Boutonnet M (2001) Appl Catal A Gen 211:239
39. Liu YY, Hayakawa T, Suzuki K, Hamakawa S, Tsunoda T, Ishii T, Kumagai M (2002) Appl Catal A Gen 223:137
40. Esposito S, Turco M, Bagnasco G, Cammarano C, Pernice P, Aronne A (2010) Appl Catal A Gen 372:48
41. Park I, Lee J, Rhee Y, Han Y, Kim H (2003) Appl Catal A Gen 253:249
42. Park I, Rhee Y, Lee J, Han Y, Jeon J, Kim H (2003) Res Chem Intermed 29:575
43. Christensen KO, Chen D, Lødeng R, Holmen A (2006) Appl Catal A Gen 314:9
44. Ereña J, Sierra I, Olazar M, Gayubo AG, Aguayo AT (2008) Ind Eng Chem Res 47:2238
45. Martín N, Viniegra M, Lima E, Espinosa G (2004) Ind Eng Chem Res 43:1206
46. Sierra I, Ereña J, Aguayo AT, Arandes JM, Bilbao J (2010) Appl Catal B Environ 94:108